Check for updates

European Journal of Neurology

european journal of neurology
the official journal of the european academy of neurology

ORIGINAL ARTICLE OPEN ACCESS

Muscle MRI Contributes to the Differential Diagnosis Between Distal Myopathies and Distal Hereditary Motor Neuropathies

María Payá[1,2,3] | Sofía Portela[1,2] | Rafael Sivera[1,2,4,5,6] | Marina Frasquet[1,2] | Fernando Más-Estellés[7] | Pilar Martí[4,5] | Inmaculada Azorín[4,5] | Karolina Aragon-Gawinska[4] | María Tárrega[8] | Herminia Argente-Escrig[1,2] | Juan F. Vázquez-Costa[1,2,4,5,9] | Roger Vilchez[4,5] | Juan J. Vilchez[1,2,4,5] | Teresa Sevilla[1,2,4,5,9] | Nuria Muelas[1,2,4,5,9]

[1]Neuromuscular Diseases Unit, Neurology Department, Hospital Universitari I Politècnic La Fe, Valencia, Spain | [2]Member of the European Reference Network for Rare Neuromuscular Diseases (ERN EURO-NMD) | [3]Instituto de Investigación Sanitaria de Castilla-La Mancha (IDISCAM), Toledo, Spain | [4]Neuromuscular and Ataxias Research Group, Instituto de Investigación Sanitaria La Fe, Valencia, Spain | [5]Centro de Investigación Biomédica en Red de Enfermedades Raras (CIBERER), Valencia, Spain | [6]Department of Medicine, Universidad CEU-Cardenal Herrera, Alfara del Patriarca, Spain | [7]Ascires, Neurorradiology Section, Área Clínica de Imagen Médica, Hospital Universitari I Politècnic La Fe, Valencia, Spain | [8]Department of Clinical Neurophysiology, Hospital Universitari i Politècnic La Fe, Valencia, Spain | [9]Department of Medicine, Universitat de València, Valencia, Spain

Correspondence: Nuria Muelas (nuria.muelas@uv.es)

Received: 3 July 2025 | **Revised:** 1 October 2025 | **Accepted:** 14 November 2025

Keywords: distal hereditary motor neuropathies | distal myopathies | muscle islands | muscle MRI | neuromyopathies

ABSTRACT

Background: Distinguishing between distal myopathies (DMs) and distal hereditary motor neuropathies (dHMNs) can be challenging because clinical, EMG and biopsy findings sometimes overlap. This study aims to identify distinctive muscle MRI features that can guide the diagnosis.

Methods: We collected clinical, genetic and muscle MRI data from patients with a confirmed diagnosis of DM and dHMN. We analyzed potential MRI characteristics to distinguish these conditions and to guide molecular diagnosis, such as the texture and pattern of infiltration.

Results: Seventy-eight (71.5%) patients diagnosed with DMs and thirty-one (28.4%) with dHMNs were included. A length-dependent pattern of muscle involvement, a distal to proximal gradient of fat replacement along the length of the muscles and severe and widespread involvement of foot muscles were more common in patients with dHMNs. Muscle hypertrophy and asymmetry were more frequently observed in the DMs. A reticular pattern of fat infiltration was exclusive to patients with dHMNs, while the moth-eaten pattern predominated in DMs. Muscle islands were more commonly identified in dHMNs (54.8%) but were also observed in 32% of patients with DMs.

Conclusions: Analysis of MRI features can help distinguish between DMs and dHMNs. A reticular pattern is an early feature of dHMNs while muscle islands are identified in advanced stages and in some forms of DMs, though not specific to neurogenic conditions. We recommend including foot muscles in the MRI protocol as they show extensive involvement in most dHMNs, while in DMs their involvement correlates with greater fatty infiltration of lower leg muscles.

María Payá and Sofía Portela are contributed equally to this work.

This is an open access article under the terms of the Creative Commons Attribution-NonCommercial-NoDerivs License, which permits use and distribution in any medium, provided the original work is properly cited, the use is non-commercial and no modifications or adaptations are made.

© 2026 The Author(s). *European Journal of Neurology* published by John Wiley & Sons Ltd on behalf of European Academy of Neurology.

1 | Introduction

Distal myopathies (DMs) and distal hereditary motor neuropathies (dHMNs) are heterogenous genetic disorders characterized by distal weakness of the upper and particularly the lower limbs [1, 2]. An increasing number of genes have been related to DMs and dHMNs, but molecular diagnosis is inconclusive in some patients, despite the implementation of next generation sequencing (NGS). This is particularly true of dHMNs, which have a low rate of genetic diagnosis (less than 50%) [3–6]. Both groups of disorders can debut at any age from childhood to adulthood and can show dominant, recessive, and X-linked patterns of inheritance, although it is not unusual to find sporadic presentations.

Differential diagnosis between DMs and dHMNs can be challenging because clinical phenotypes tend to overlap. Electromyographic and histopathological features can help determine whether the etiology is neurogenic or myopathic, but findings in the mentioned techniques can also overlap in some cases, making diagnosis even more complicated. Moreover, a growing list of genes causing either DMs, dHMNs or other neurogenic phenotypes has been identified, such as the heat shock protein (HSP) family or VCP, and the term neuromyopathies has emerged [7, 8].

Muscle magnetic resonance imaging (MRI) can identify muscle involvement patterns that guide diagnosis and has therefore become a powerful tool in the evaluation of patients with neuromuscular disorders. Specific patterns of muscle involvement have been identified in several DMs and to a lesser extent in the most common subtypes of dHMNs [3, 9–12]. MRI also plays an increasingly important role in monitoring disease progression and therapeutic response in clinical trials [13, 14].

To our knowledge, only one study that addressed distinguishing MRI features between myopathic and neurogenic disorders has so far been published [15]. The authors focused on patients with early onset distal weakness and concluded that the presence of muscle islands, described as small areas of muscle tissue with normal signal intensity surrounded by areas with similar intensity to subcutaneous fat, is the main distinguishing feature of neurogenic disorders. This signature has 100% diagnostic accuracy, being clearly superior to EMG and muscle biopsy findings. However, the study included a small number of patients and diagnosis was not confirmed genetically in all cases, making the findings difficult to extrapolate. The authors also reviewed muscle MRI scans from other published studies reporting the presence of islands in patients with diverse neurogenic conditions [15]. Besides, a recent study of a large cohort of dHMN patients evaluated with MRI concluded that muscle islands are a distinctive feature of neurogenic conditions, as well as the presence of a reticular pattern of fat replacement in early stages [10]. None of these studies evaluated the involvement of the intrinsic foot muscles.

The aim of this study is to identify distinguishing MRI features between DMs and dHMNs that can help the diagnostic process and guide molecular diagnosis of patients with distal weakness. We also analyze the contribution of assessing foot muscle involvement and determine whether muscle islands and a reticular pattern of fat infiltration are distinctive findings that are exclusive to dHMNs.

2 | Patients and Methods

2.1 | Patients and Study Design

Patients diagnosed with DMs and dHMNs in a neuromuscular reference centre (NMRC) were reviewed. We recruited for the study patients that had a molecular diagnosis of either DM or dHMN obtained by standard genetic testing [4, 16] and that had muscle MRI scans available for assessment.

The study was approved by our Institutional Ethics Committee and written informed consent was obtained from each patient, in accordance with the Declaration of Helsinki.

We reviewed electronic records to collect demographic and clinical data, including gender, age at disease onset, age at muscle imaging, disease duration, molecular diagnosis, and functional disability. Due to the lack of standardized scales applied to both DMs and dHMNs, functional disability was categorized based on gait impairment: mild (abnormal gait but unassisted), moderate (unilateral support required), and severe (bilateral support or wheelchair use).

2.2 | Muscle-Imaging Studies and Analysis

All muscle MRI scans were performed according to the previously described protocol using T1 weighted spin echo (T1w) and T2 weighted short-tau inversion recovery (STIR-T2w) sequences in axial non-contiguous sections [17]. Two authors blinded to the molecular diagnosis analyzed the scans of the pelvis, thighs and lower legs in all patients. Foot muscles were analyzed in 62 patients because their MRI protocol included this region. Fat infiltration of each muscle was evaluated using the Mercuri score modified by Fischer [18]. A median whole cumulative score (WCS) was calculated for each patient, and a median score was calculated for each anatomic segment (pelvis, thighs, and lower legs) in each patient by summing the scores of the individual muscles and taking into account the muscles included in the segment. The WCS was normalized by calculating the median in case of missing muscles which happened only in a minority of cases. A distal-to-proximal gradient of muscle involvement was defined as ≥ 1 point difference in the Mercuri score between distal and proximal regions of the muscle. Asymmetric involvement was considered when there was ≥ 2 point difference between sides in at least one muscle. The presence of a length-dependent pattern of muscle involvement was determined by comparing the median fat infiltration scores of muscles in three lower limb regions: distal (lower leg), middle (thigh), and proximal (pelvis). Foot muscles were not included because they were not available in all patients. Muscle atrophy and hypertrophy were evaluated by comparing the volume of affected muscles with other preserved muscles in the same region. STIR images were reviewed and classified as positive (increased signal intensity) or negative (no increased signal). Muscle texture was

14681331, 2026, 1, Downloaded from https://onlinelibrary.wiley.com/doi/10.1111/ene.70456 by Spanish Cochrane National Provision (Ministerio de Sanidad), Wiley Online Library on [13/03/2026]. See the Terms and Conditions (https://onlinelibrary.wiley.com/terms-and-conditions) on Wiley Online Library for rules of use; OA articles are governed by the applicable Creative Commons License

analyzed by inspection considering three patterns of fat infiltration (moth-eaten, washed-out, and reticular) as well as the presence of muscle islands [19] defined as areas of muscle tissue embedded in areas of fatty infiltration, taking care to avoid confusing them with vascular or tendon structures.

2.3 | Statistics

Categorical variables are presented as counts and percentages, while quantitative variables are expressed as median (IQR) or mean (SD), based on their distribution, and were assessed using the Shapiro–Wilk test. Clinical and radiological findings were compared between groups using Fisher's exact test for categorical variables, Student's *t*-test for normally distributed continuous variables, and the Mann–Whitney *U* test for non-normally distributed variables. Hierarchical analysis and heatmap visualizations of muscle fat infiltration scores, along with statistical analyses, were performed using R software (http://www.r-project.org). Density plots were created to show patient distribution based on functional disability and WCS scores, while boxplots represented the degree and distribution of fat replacement in muscles from the anterior and posterior compartments of the lower legs and thighs. Boxplots were generated using the R package *ggplot2*, where the upper whisker corresponds to the minimum between the maximum observed value and $Q3 + 1.5 \times IQR$, and the lower whisker corresponds to the maximum between the minimum observed value and $Q1 - 1.5 \times IQR$.

Spearman's rank correlation was used (coefficient reported as ρ) to investigate correlations between gait impairment and disease duration with the degree of muscle fat infiltration by MRI (WCS). The correlation was considered significant if the *p*-value was less than 0.05 and ρ was 0.6 or higher.

3 | Results

3.1 | Patient Characteristics and Genetic Diagnosis

One hundred and nine patients were enrolled; 78 (71.5%) were diagnosed with DMs and 31 (28.4%) with dHMNs. Patients with different molecular subtypes were included, the most prevalent being related to *MYH7* (36.7%) and *ANO5* (13.8%) pathogenic variants in the DMs cohort, and to *HSPB1* (8.2%) and *BICD2* (8.2%) variants in the dHMNs. The main characteristics of both groups are summarized in Table 1. The dHMN subgroup had a higher proportion of men (67.7%), while the proportion of men and women was similar in the DMs; however, this difference was not statistically significant ($p = 0.17$). Median age at disease onset was similar in both cohorts: 18 years (5.2–34.7) in DMs and 18.5 years (6–40) in dHMNs. However, age at muscle imaging was significantly higher in DMs compared to dHMNs (45.2 vs. 36.3 years, respectively; $p = 0.01$).

Gait impairment severity differed between groups ($p = 0.003$): in the DMs group, 43.6% had mild, 37.2% moderate, and 8.9% severe gait impairment, while 77.4% of the dHMNs cohort had mild gait impairment, whereas 6.4% had moderate and 6.4% had severe impairment. Eleven patients (10%) were asymptomatic. Of these, eight carried *ANO5* variants, two carried *BICD2* variants and one carried *HSPB1* variants.

Table S1 shows the clinical, molecular and muscle imaging data from each patient of the cohort.

3.2 | Muscle-Imaging Features

Twenty-five muscles were evaluated from pelvis and lower limbs scans in all patients. Table S2 shows the degree of muscle fat replacement indicating Mercuri score for each individual muscle, together with the median Mercuri score of different anatomical regions (lower leg, thigh and pelvis) and median WCS in each patient. All patients, except for one asymptomatic carrier of the p. Arg140Gly variant in *HSPB1*, presented muscle abnormalities on MRI. Table S3 shows the median Mercuri score of each muscle and anatomical region (lower leg, thigh, and pelvis) of patients in the DMs and dHMNs groups. Overall, there were no significant differences in the median Mercuri lower legs score between both cohorts; however, the distribution varied, with involvement of the posterior compartment of the leg (gastrocnemius medial –GM–, gastrocnemius lateral –GL–, and soleus –SL–) being predominant in dHMNs (Figure 1A). The distribution of fat infiltration was more heterogeneous in DMs, but an overall predilection for the anterior compartment of the lower leg (Figure 1A) and the posterior compartment of the thighs (Figure 1B) was observed. The adductor magnus (AM) and adductor longus (AL) muscles were more often involved in DMs than in dHMNs. The rectus femoris (RF), usually preserved in DMs, was frequently involved in dHMNs. Thighs and pelvis muscles showed higher median Mercuri scores in DMs than in dHMNs, but these differences were not statistically significant. The gluteus minimus (GMm) was more involved than the gluteus maximus (GMa) in DMs, while the gluteus medius (GMe) and GMm were predominantly involved in dHMNs.

A length-dependent pattern of muscle involvement was observed in a large proportion of patients with dHMNs (63.3%) and was somewhat less frequent in DMs (46.1%) (this difference was not statistically significant ($p = 0.17$)). This pattern was found in all patients with pathogenic variants in *GNE* (Figure 2A–D), *GARS1* (Figure 2E–H), *SOD1* and *DNAJB2/HSJ1*; in 67% of patients with pathogenic variants in *HSPB1*; in 50% of patients with pathogenic variants in *ANO5*, *MYH7.* and *DYSF*; in 44% of patients with pathogenic variants in *BICD2*; and in 25% of patients with pathogenic variants in *MYOT*. We did not observe a length-dependent pattern in any patient with variants in *TTN* or *DYNC1H1*.

Foot muscles were evaluated in 62 patients, 22 with dHMNs and 40 with DMs, and showed involvement in 45.2% of cases. Foot muscle involvement was more frequent and severe in dHMNs (68.2%) compared to DMs (32.5%, $p = 0.01$) (median Mercuri score 2.25 (IQR 1.25–3) in dHMNs vs. 1.25 (IQR 0.5–2) in DMs; $p = 0.25$). The pattern of foot muscle involvement was usually widespread in both cohorts (Figure 3G,I,L), but in general, dHMNs exhibited more diffuse fat replacement (80% vs. 50% in DMs; $p = 0.25$). Foot muscle involvement was observed in all patients with *HSPB1*, *GARS1*, *DNAJB2*, and *SOD1* pathogenic variants who underwent foot scans. In contrast, no patients with

14681331, 2026, 1, Downloaded from https://onlinelibrary.wiley.com/doi/10.1111/ene.70456 by Spanish Cochrane National Provision (Ministerio de Sanidad), Wiley Online Library on [13/03/2026]. See the Terms and Conditions (https://onlinelibrary.wiley.com/terms-and-conditions) on Wiley Online Library for rules of use; OA articles are governed by the applicable Creative Commons License

TABLE 1 | Patient demographics and main imaging features in distal myopathies (DMs) and distal hereditary motor neuropathies (dHMNs).

	Distal myopathies $N = 78$ (71.5%)	Distal hereditary motor neuropathies $N = 31$ (28.4%)
Sex male, *n* (%)	40 (51.3%)	21 (67.7%)
Age		
At onset (years), Median (Q1–Q3, IQR)	18 (5.2–34.7, 29.5)	18.5 (6–40, 34)
At MRI (years), Median (Q1–Q3, IQR)* ($p = 0.01$)	44.5 (36–58.2, 22.2)	35 (22–49.5, 37.5)
Disease duration at MRI (years), Median (Q1–Q3, IQR)* ($p = 003$)	19 (9.2–36, 26.7)	9 (3.7–19.2, 15.5)
Asymptomatic at MRI, *n* (%)	8 (10.2%)	3 (9.7%)
Functional gait impairment, *n* (%)		
Mild	34 (43.6%)	24 (77.4%)
Moderate	28 (37.2%)	2 (6.4%)
Severe	7 (8.9%)	2 (6.4%)
Molecular diagnosis, *n* (%)	MYH7: 40 (36.7%) ANO5: 15 (13.8%) DYSF: 8 (7.3%) TTN: 7 (6.4%) MYOT: 4 (3.7%) GNE: 4 (3.7%)	BICD2: 9 (8.2%) HSPB1: 9 (8.2%) DYNC1H1: 4 (3.7%) GARS1: 4 (3.7%) DNAJB2/HSJ1: 3 (2.7%) SOD1: 2 (1.8%)
Median Mercuri Score, Me (Q1–Q3, IQR)		
Pelvis (glutei)	1 (0–2, 2)	0.7 (0–1.8, 1.8)
Thighs	1.4 (0.4–2.1, 1.6)	0.8 (0.3–1.7, 1.4)
Lower legs	1.4 (0.9–2.1, 1.3)	1.5 (0.8–2.15, 1.35)
Foot muscles evaluated, *n* (%)	40	22
Fat infiltration of foot muscles, *n* (%)* ($p = 0.01$)	13 (32.5%)	15 (68.2%)
Median Mercuri Score of foot, Me (Q1–Q3, IQR)	1.25 (0.5–2, 1.5)	2.25 (1.25–3, 1.75)
Distal to proximal gradient of fat replacement on MRI		
Thighs, *n* (%)	7 (9.0%)	10 (33.3%)
Lower leg, *n* (%)	11 (14.1%)	14 (46.7%)
Length-dependent pattern of muscle involvement on MRI, *n* (%)	36 (46.1%)	19 (63.3%)
Asymmetric MRI involvement, *n* (%)* ($p = 0.005$)	35 (44.9%)	4 (13.3%)
Muscle atrophy on MRI, *n* (%)	39 (50.6%)	14 (45.2%)
Muscle hypertrophy on MRI, *n* (%)* ($p = 0.002$)	57 (73.1%)	12 (38.7%)
STIR hyperintensities on MRI, *n* (%)	44 (59.4%)	16 (53.3%)
Predominant muscle texture on MRI, *n* (%)	Moth-eaten 59 (75.6%) Wash-out 19 (24.4%)	Moth-eaten 8 (26.7%) Reticular 22 (73.3%)
Presence of muscle islands, *n* (%)* ($p = 0.048$)	24 (32.0%)	17 (54.8%)
Muscle islands by molecular diagnosis, *n* (%)	MYH7: 11 (27.5%) ANO5: 2 (13.3%) DYSF: 3 (50%) TTN: 3 (42.8%) MYOT: 3 (75%) GNE: 2 (50%)	BICD2: 9 (100%) HSPB1: 2 (22.2%) DYNC1H1: 3 (75%) GARS1: 2 (50%) DNAJB2/HSJ1: 0 (0%) SOD1: 1 (50%)

Note: Statistically significant differences ($p < 0.05$) are marked with an asterisk.

14681331, 2026, 1, Downloaded from https://onlinelibrary.wiley.com/doi/10.1111/ene.70456 by Spanish Cochrane National Provision (Ministerio de Sanidad), Wiley Online Library on [13/03/2026]. See the Terms and Conditions (https://onlinelibrary.wiley.com/terms-and-conditions) on Wiley Online Library for rules of use; OA articles are governed by the applicable Creative Commons License

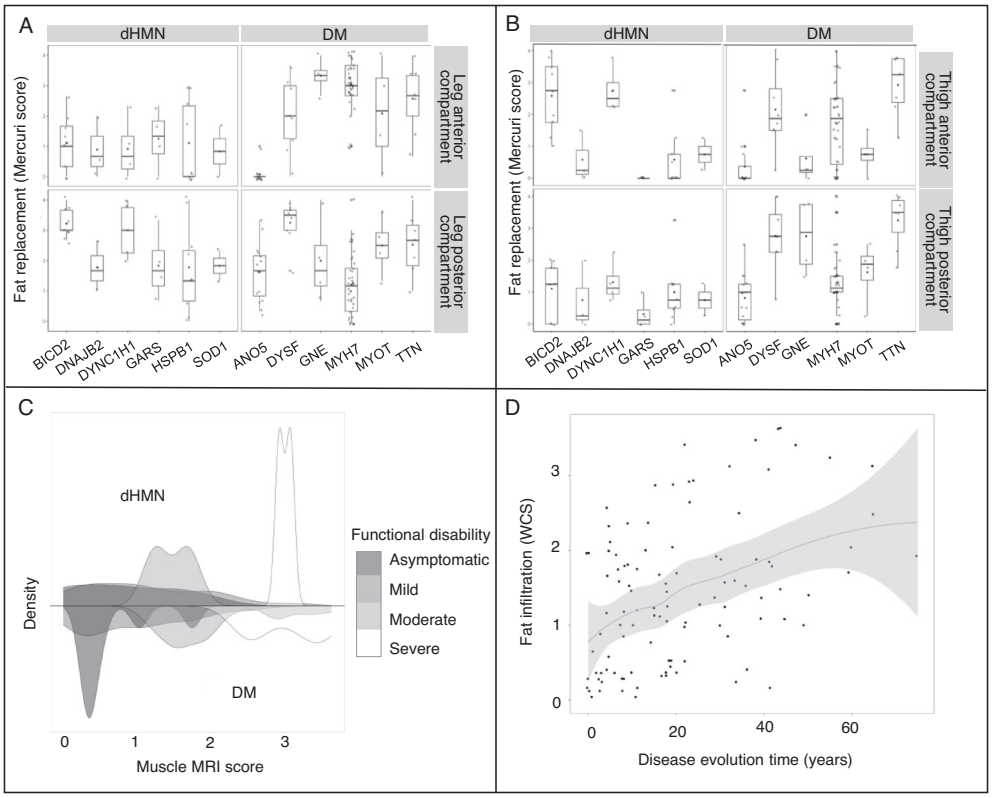

FIGURE 1 | Boxplot showing the degree of fat replacement (median WCS) in muscles of the anterior and posterior compartments of the lower leg† (A) and thigh (B) clustering by groups (dHMN, DM) and molecular diagnosis. The central line within each box represents the median value, the central square represents the mean, the edges of the box represent the first and third quartiles (IQR). (C) Density plot showing the distribution of patients according to their median MRI whole cumulative score (WCS) and functional disability. Most of asymptomatic patients (dark gray) had a median WCS between 0 and 1; patients with moderate disability (medium gray) had a median WCS between 1 and 2; and patients with severe disability (white) had higher WCS (> 2). (D) Scatter plot with a regression line showing a positive correlation between the degree of muscle fat replacement (median WCS) and disease duration (years) of the patients of the cohort. The regression line was fitted using the loess method (locally estimated scatterplot smoothing) implemented in ggplot2; the shaded area represents the standard error of the regression. †Muscles included in the leg anterior compartment: Tibialis anterior (TA), extensor digitorum longus (EDL), extensor hallucis longus (EHL) and in the leg posterior compartment: Gastrocnemius medial (GM), gastrocnemius lateral (GL) and soleus (SL). ¶Muscles included in the thigh anterior compartment: Vastus medialis (VM), vastus intermedius (VI), vastus lateralis (VL), rectus femoris (RF), and in the thigh posterior compartment: Semimembranosus (SM), semitendinosus (ST) and biceps femoris (BF).

DYNC1H1 variants showed foot muscle involvement. In the DMs cohort, fat infiltration of foot muscles was mainly related to variants in *GNE* (Figure 3D) and *MYOT* (Figure 3E). A correlation between higher WCS and foot muscle involvement was observed in the DMs cohort ($p < 0.001$) but not in the dHMNs. Higher median Mercuri scores in the lower leg were associated with foot muscle involvement in the overall series ($p = 0.008$), and specifically in the DM cohort ($p < 0.001$), but not in the dHMNs.

Fat replacement along the length of the muscles following a distal to proximal gradient was observed in 34 patients (31.5%) and was more common in dHMNs than in DMs (54.8% vs. 21.8%, respectively; $p < 0.01$). This gradient was predominant in the lower legs (Figure 4C,D,H,I,M,N) compared to the thighs (Figure 4A,B,F,G,K,L) in both cohorts. In DMs, it was mainly related to *ANO5* (Figure 4A–E), *DYSF* (Figure 4K,L) and *MYH7* pathogenic variants (involving the thighs in 9.0% and the legs in 14.1%). In patients with dHMNs, this gradient was observed in all patients with variants in *DYNC1H1* (75% in thighs and 25% in the legs) and 78% of patients with *HSPB1* mutations (67.7% in the legs and 44.4% in the thighs) (Figure 4F–I).

Of note, while patients with *DYNC1H1* mutations exhibited a distal to proximal gradient but not a length-dependent pattern, patients with *HSPB1* variants tended to show both. In patients with *BICD2* pathogenic variants, a length-dependent pattern was observed at 44% while the distal to proximal gradient was less common (22%).

Asymmetric involvement was more common in the DMs cohort vs. the dHMNs (44.9% vs. 13.3% respectively; $p = 0.004$). In DMs, it was mainly associated with *DYSF* (62.5%), *GNE* (50%), *MYOT* (50%), *MYH7* (45%), *TTN* (43%) and *ANO5* (30%). Asymmetry was also observed in 50% of patients with *SOD1* pathogenic variants, 25% with *DYNC1H1*, and 11% with *BICD2* and *HSPB1* variants.

Muscle hypertrophy was also a distinguishing feature between both groups, being more frequently observed in the DMs cohort than in the dHMNs (73.1% vs. 38.7%; $p = 0.0017$). It was mainly associated with variants in *ANO5* (100%), *TTN* (100%), *GNE* (75%), *MYOT* (75%), *DYSF* (75%) (Figure 4K,L), and *MYH7* (57.5%). In the dHMNs cohort, muscle hypertrophy predominated in

14681331, 2026, 1, Downloaded from https://onlinelibrary.wiley.com/doi/10.1111/ene.70456 by Spanish Cochrane National Provision (Ministerio de Sanidad), Wiley Online Library on [13/03/2026]. See the Terms and Conditions (https://onlinelibrary.wiley.com/terms-and-conditions) on Wiley Online Library for rules of use; OA articles are governed by the applicable Creative Commons License

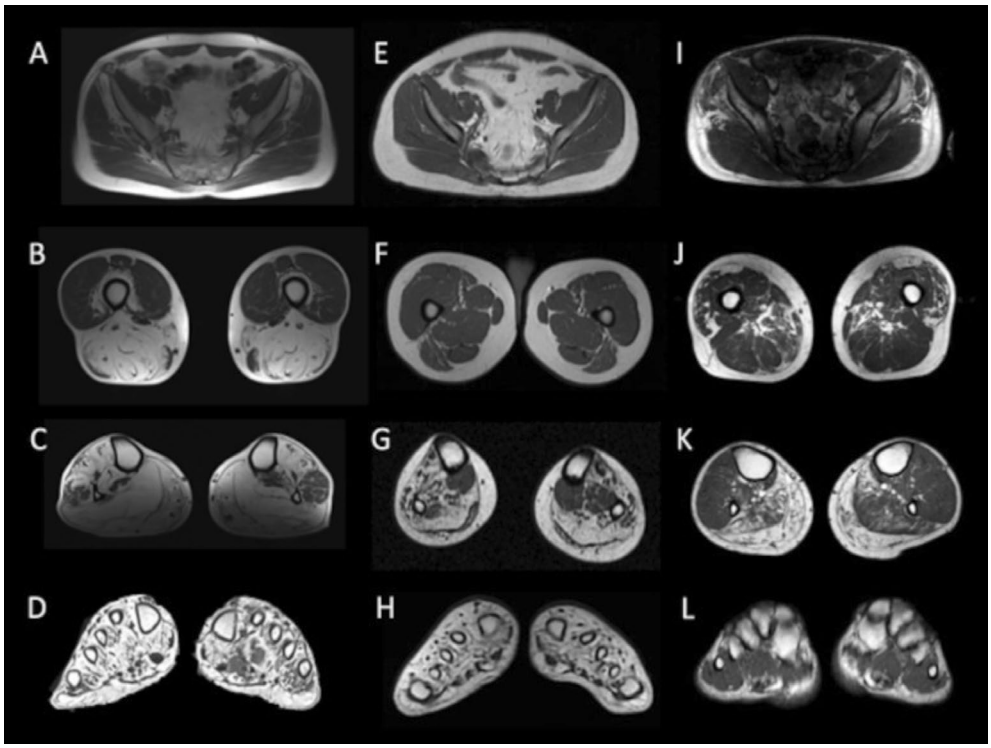

FIGURE 2 | Length-dependent pattern of muscle involvement. A length-dependent pattern was observed in patients with *GNE* variants (A–D) and *GARS1* (E–H) variants, but not in patients with *DYNC1H1* variants (I–L). A preferential involvement of foot and lower leg muscles was noted in *GARS1* patients (E–H), while foot muscles were preserved in the patient with a *DYNC1H1* variant (L), contrasting with the infiltration of muscles of the thigh, pelvis, and lower legs (I–K).

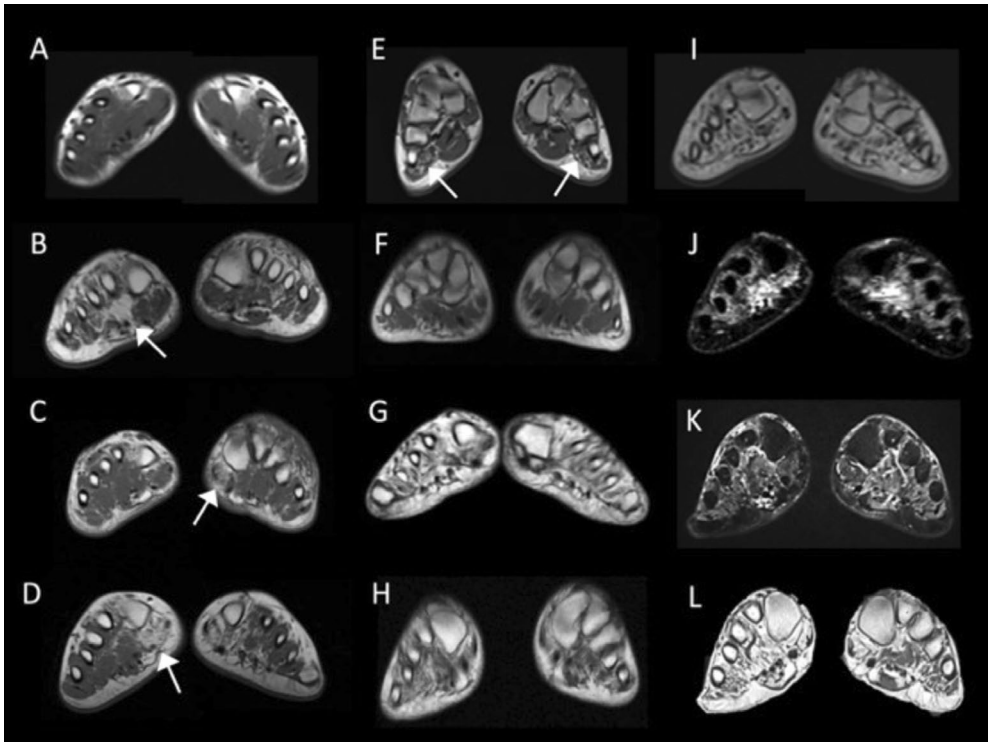

FIGURE 3 | MRI scans showing variable involvement of foot muscles in DMs and dHMNs. Foot muscle preservation (A) and asymmetrical involvement (B; arrow) in 2 patients with Laing myopathy. Focal and asymmetric fat replacement in the medial compartment in patients with BICD2 (C; arrow) and GNE (D; arrow) variants. (E) Shows mild involvement of the lateral compartment (arrow) in a patient with myotilinopathy. Foot muscles were usually preserved in patients with BICD2 variants (F), but were frequently involved in HSPB1 (G), SOD1 (H), DNAJB2 (I) and GARS1 (Figure 2) variants. STIR hyperintensities were observed in foot muscles as shown in (J), which corresponds to a patient with HSPB1 and (K) to a patient with GNE variants. Foot muscle infiltration was observed in some DMs, particularly in patients with variants in GNE (D, L) and MYOT.

14681331, 2026, 1, Downloaded from https://onlinelibrary.wiley.com/doi/10.1111/ene.70456 by Spanish Cochrane National Provision (Ministerio de Sanidad), Wiley Online Library on [13/03/2026]. See the Terms and Conditions (https://onlinelibrary.wiley.com/terms-and-conditions) on Wiley Online Library for rules of use; OA articles are governed by the applicable Creative Commons License

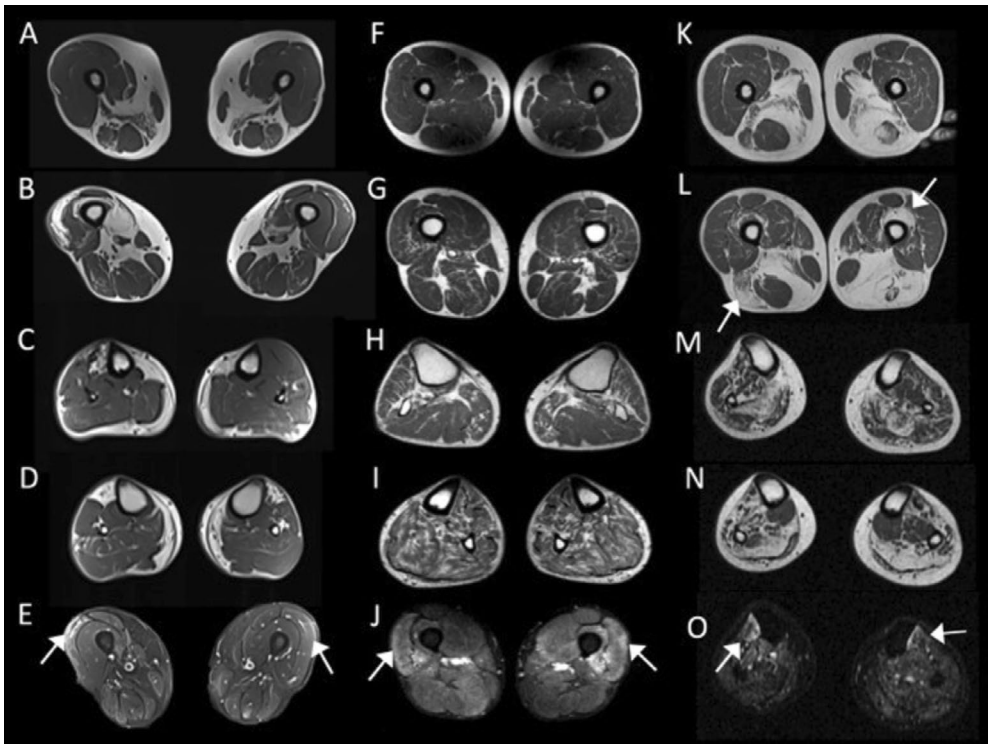

FIGURE 4 | Distal-to-proximal gradient of fat replacement along the length of the muscles and STIR hyperintensities in patients with dHMNs and DMs. (A–D) T1-weighted MRI scans showing preferential involvement of the distal portions of the vasti (A, B), tibialis anterior, and gastrocnemius medialis (C, D) and (E) STIR enhancement in the vasti (arrow) in a patient with *ANO5* pathogenic variants. (F–J) A distal-to-proximal gradient of fat replacement in the thighs (F, G) and lower leg muscles (H, I) and STIR hyperintensities in the distal portions of the vasti (J, arrow) in a patient with the p.Arg140Gly *HSPB1* variant; a reticular pattern of fat replacement is also observed (H, I). (K, L) shows preferential involvement of the distal portions of the vastus intermedius and biceps femoris (arrows), along with hypertrophy of the sartorius and gracilis in a patient with *DYSF* variants. (M, N) A patient with the p.Ser265*Phe GARS1* variant exhibited a distal-to-proximal gradient of atrophy and fat replacement with a reticular pattern (M, N); STIR hyperintensities are also observed (O).

patients with variants in *BICD2* (55.5%), *DYNC1H1* (50%), and *HSPB1* (44%), while no patients with *GARS1* or *DNAJB2* variants exhibited this feature.

Muscle atrophy was also observed (Figure 4M,N), being prominent in around half of the overall cohort.

STIR hyperintensities were observed in 60 patients overall (57.7%); occurrence was similar in both DMs and dHMNs cohorts (59.4% vs. 53.3%, respectively). The distribution of STIR hyperintensities varied depending on the pattern of muscle involvement specific to each condition, so the pattern of edema was useful for differentiating particular conditions (Figure 4E,J,O).

3.3 | Texture and Muscle Islands

A reticular pattern of fatty replacement was observed in 73.3% of patients with dHMNs (Figure 5A–D) while the moth-eaten pattern predominated in DMs (75.6%; Figure 5G,H) followed by the wash-out pattern (24.4%; Figure 5I–L).

Muscle islands were more frequently identified in patients with dHMNs vs. DMs (54.8% vs. 32%, respectively; $p = 0.048$). The number of muscles with islands and their distribution was variable (Table S4). Muscle islands were found in all patients with pathogenic variants in *BICD2* (Figure 5E,F), in 75% of patients with *DYNC1H1* variants (Figure 5A,B), in 50% with *GARS1* and *SOD1* variants, and in 22% of patients with *HSPB1* variants. We did not identify muscle islands in any patient with *DNAJB2/HSJ1* variants. In the DMs, muscle islands were observed in patients with variants in *MYOT* (75%) (Figure 5I,J), *GNE* (50%) (Figure 5K,L), and *TTN* (43%), and were less frequently associated with *MYH7* (27.5%) and *ANO5* (13%) variants. The presence of muscle islands correlated with a higher degree of fat infiltration (Spearman's $p = 0.56$; $p < 0.001$), being exceptional when the Mercuri score was ≤ 2.

3.4 | MRI Pattern According to the Affected Gene

Muscle involvement of the patients grouped by molecular diagnosis is represented in a heatmap (Figure 6) that shows characteristic patterns (Appendix S1), most of which are consistent with previous studies. The pattern was not well defined in patients with variants in *TTN* due to variable distribution of fat replacement, but the flexor hallucis longus (FHL) and tibialis posterior (TP) muscles, typically preserved in myopathies, were frequently involved. Although we only included a small number of patients with variants in *DNAJB2* and *SOD1* in this study, a predilection for the posterior leg compartment (SL > GM > GL, and also P and FHL) and posterior and lateral leg compartments (SL and PL), respectively, was observed, with the thighs and pelvic muscles being preserved in early stages.

14681331, 2026, 1, Downloaded from https://onlinelibrary.wiley.com/doi/10.1111/ene.70456 by Spanish Cochrane National Provision (Ministerio de Sanidad), Wiley Online Library on [13/03/2026]. See the Terms and Conditions (https://onlinelibrary.wiley.com/terms-and-conditions) on Wiley Online Library for rules of use; OA articles are governed by the applicable Creative Commons License

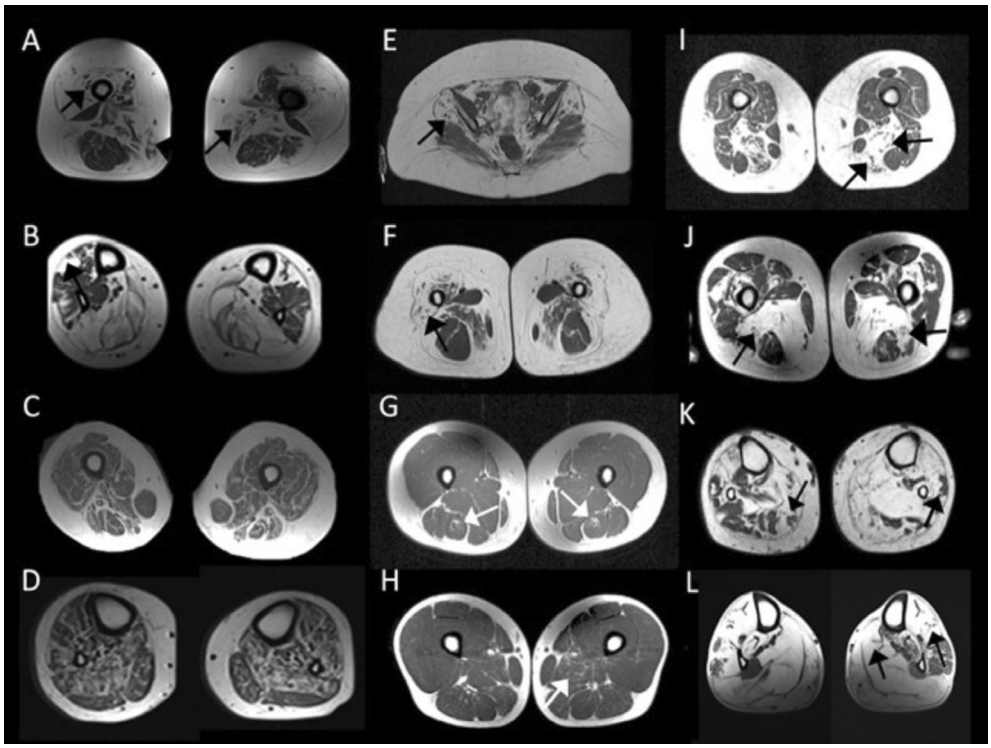

FIGURE 5 | Texture of fat replacement and islands. (A, B) shows muscle islands (arrows) and a reticular pattern in thighs and lower leg muscles in a patient with a *DYNC1H1* variant. Diffuse reticular pattern affecting muscles of the thighs (C) and lower legs (D) in a patient with a *DNAJB2* variant. (E, F) muscle islands in gluteus minimus and medius (E), vasti, rectus femoris and biceps femoris (F) in a patient with a *BICD2* variant; quadriceps atrophy contrasting with adductor longus and semitendinosus hypertrophy of is also observed (F). Patients with DMs had a moth-eaten pattern of fat replacement (arrow) in early stages (G, H) progressing to wash-out patterns (I–L); muscle islands (arrow) were identified in some patients with DMs as shown in (I–L); (G) corresponds to a patient with mutations in *GNE*, (H) to a patient with *ANO5*-myopathy, (I, J) to patients with variants in *MYOT*, and (K, L) to a patient with *GNE* variants.

3.5 | Correlation Between MRI Findings and Clinical Data

Figure 1C shows the distribution of patients, their median WCS and functional disability. We found a statistically significant correlation between WCS and functional disability (Spearman's $\rho = 0.64$; $p < 0.001$). Note that all but one asymptomatic patient had a median WCS <1; most had *ANO5* biallelic variants. Patients with moderate disability had a median WCS of 1–2, and those with severe disability had higher Mercuri scores (>2). We also observed a positive correlation between the degree of fat replacement and disease duration (Spearman's $\rho = 0.40$; $p < 0.001$) (Figure 1D).

4 | Discussion

In this study, we analyzed data from a large series of patients with DMs and dHMNs, confirmed by molecular diagnosis and applying the same MRI analysis protocol that allows us to draw important conclusions. First, we identified certain imaging features that can help distinguish DMs and dHMNs, but none of them is specific except the reticular pattern of fat infiltration, exclusively found in dHMNs, while DMs exhibited moth-eaten and wash-out patterns. Therefore, the texture needs to be analyzed in order to identify different patterns of muscle fat infiltration. However, in very early stages of dHMNs the reticular pattern could not be detected as it happened in some patients of our dHMNs cohort which showed a moth-eaten pattern that prevented us from differentiating them from those with DMs. Muscle islands, reported as a signature of neurogenic conditions [10, 15] were found in 32% of our patients with DMs, showing that they are not specific to dHMNs, although they were more frequently found in this cohort (54.8%). In previous studies, muscle islands were detected in up to 79% of patients with dHMNs [10]. In Astrea et al. they were observed in all neurogenic patients but were absent in patients with distal myopathies [15], leading the authors to hypothesize that muscle islands represent the giant motor units noted on EMG in these conditions. In our DMs cohort, muscle islands were predominantly associated with *MYOT, GNE* and *TTN* variants, a finding not previously reported. However, both muscle islands and "fat pockets" have been associated with VCP-related myopathies and neutral lipid storage disease (NLSD) [20, 21], reflecting the combination with neurogenic involvement also observed in biopsies of VCP-related myopathies. Our study shows that muscle islands can be observed in some DMs in which neurogenic involvement has not been described; therefore, further studies are required to clarify their pathogenesis. Regarding dHMNs we found muscle islands in all patients with variants in *BICD2*, in line with another study reporting this finding [11]. They were also common in patients with *GARS1* variants, a finding reported [22] but also associated with *DYNC1H1* and *SOD1* variants, which to our knowledge has not previously been reported. We also confirmed that muscle islands correlated with a higher degree of fat replacement, as has been suggested elsewhere [15]. This is why muscle islands are

14681331, 2026, 1, Downloaded from https://onlinelibrary.wiley.com/doi/10.1111/ene.70456 by Spanish Cochrane National Provision (Ministerio de Sanidad), Wiley Online Library on [13/03/2026]. See the Terms and Conditions (https://onlinelibrary.wiley.com/terms-and-conditions) on Wiley Online Library for rules of use; OA articles are governed by the applicable Creative Commons License

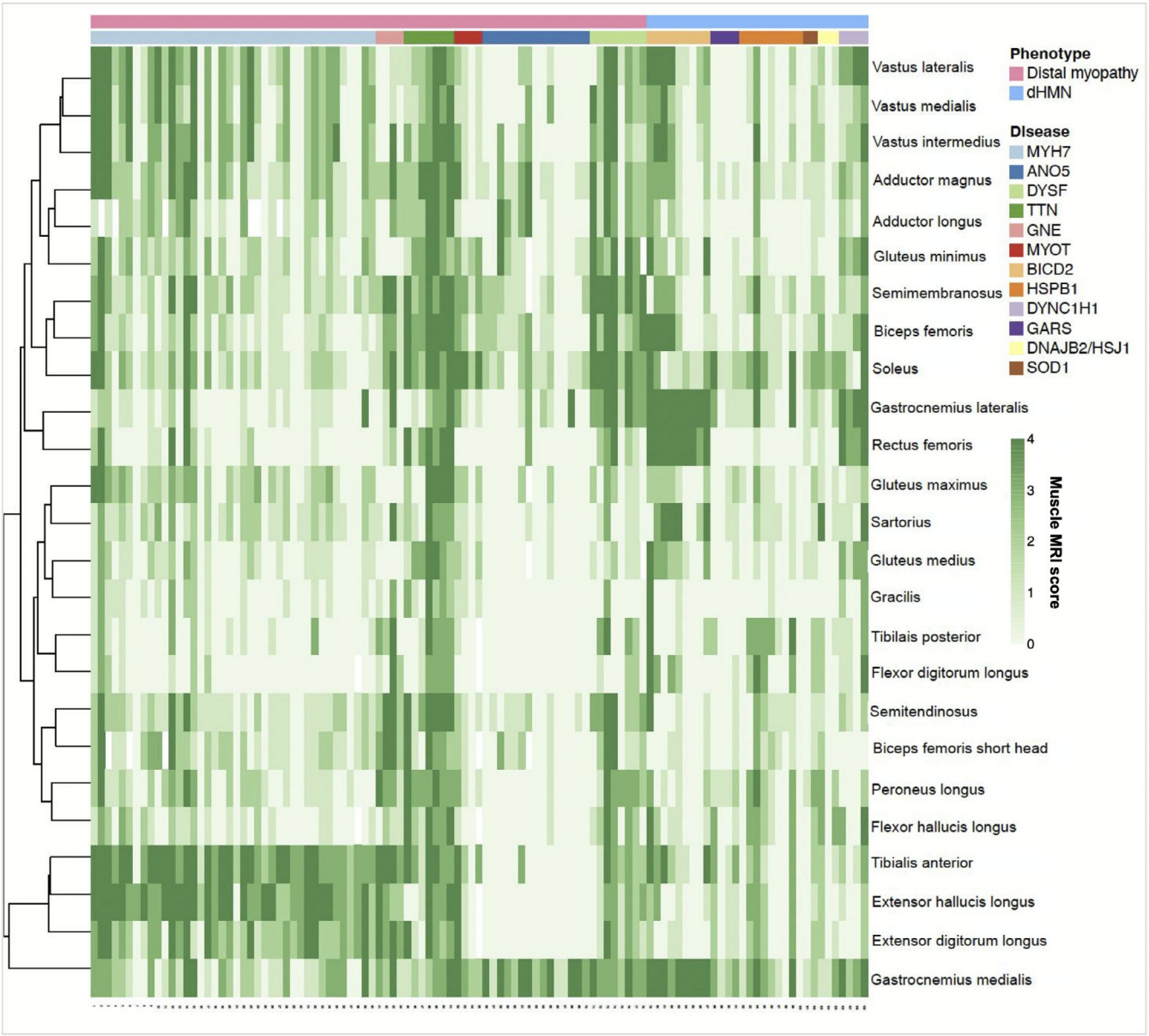

FIGURE 6 | Heatmap showing fat replacement of muscles of the leg, thigh and pelvis in patients with dHMNs and DMs. Patients and muscles are ordered according to hierarchical clustering. The Mercuri score of each muscle is indicated by different shades of green. Two rows are included at the top of the heatmap. The first-row, groups patients by phenotype (DMs vs. dHMN), while the row below groups them according to molecular diagnosis. Patterns of involvement related to specific molecular diagnosis are detailed in Appendix S1.

not found in early stages, unlike the reticular pattern which is a hallmark of neurogenic disorders [7, 12].

A length-dependent pattern of muscle infiltration was more frequently observed in dHMNs, but it was also found in patients with DMs. The difference in incidence was not statistically significant, so this feature in isolation was not useful in the differential diagnosis. It is interesting to note that patients with pathogenic variants in *GARS1*, *SOD1*, *DNAJB2/HSJ1* and *HSPB1* frequently presented a length-dependent pattern, while only 44% of patients with *BICD2* variants and none with *DYNC1H1* variants presented this feature. This is because, as previously reported, both conditions have significant proximal involvement [11, 23–25]. Regarding DMs, all patients with *GNE*-myopathy and half of all patients with *ANO5, MYH7* and *DYSF* variants, showed a length-dependent pattern [26].

We found that fat infiltration of intrinsic foot muscles was more frequent, diffuse and severe in dHMNs, while in DMs it was associated with higher WCS and higher median Mercuri score in legs muscles, suggesting that it could be a distinguishing feature between myopathic and neurogenic conditions. Analysis of foot muscle involvement has begun to be used in CMT1A, and it could become a biomarker in future clinical trials [27, 28], but it has not been applied in other neurogenic or myopathic conditions apart from Laing myopathy and *GARS1*-associated dHMN [17, 22]. In view of these results, we recommend including foot level in the MRI protocol to analyze foot muscle involvement.

A distal to proximal gradient of fat replacement along the muscles was not a specific feature, as previously reported [15], although it was more common in patients with dHMNs, especially affecting the lower legs. This distal to proximal gradient has

14681331, 2026, 1, Downloaded from https://onlinelibrary.wiley.com/doi/10.1111/ene.70456 by Spanish Cochrane National Provision (Ministerio de Sanidad), Wiley Online Library on [13/03/2026]. See the Terms and Conditions (https://onlinelibrary.wiley.com/terms-and-conditions) on Wiley Online Library for rules of use; OA articles are governed by the applicable Creative Commons License

been observed in the thighs in patients with *HSPB1* mutations [29] and also in almost half of all patients with dHMNs included in a recent study [10]. We also observed a distal to proximal gradient in 22% of the DMs patients affecting the lower legs and thighs, and mainly associated with variants in *ANO5, DYSF* and *MYH7*. This has been described in the quadriceps in patients with *ANO5* variants [30] but not in the GM, as we also observed. Regarding Laing myopathy, we have already described this feature in leg and thigh muscles [17]. This distal to proximal gradient has also been reported in *VCP* variants, mainly involving the quadriceps and soleus [21], and in sporadic Inclusion Body Myositis (sIBM) in the quadriceps [31], in contrast to the proximodistal gradient of involvement of vasti muscles described in sarcoglycanopathies and Pompe disease [32, 33].

The pattern of muscle involvement also varied between groups, with the superficial posterior compartment of the lower legs being mainly affected in the dHMNs (GM > GL > SL). Patients with DMs showed a more heterogeneous pattern, but fat replacement predominantly affected the anterior compartment of the legs, followed by GM > SL. This may be due to bias, as over one-third of our cohort presented Laing myopathy, a disease characterized by preferential involvement of the anterior leg.

Asymmetric involvement was observed in nearly half of patients with DMs but was rare in our dHMNs cohort (13.3%), while in a previous study it was described in up to 29% of dHMN patients [10]. Asymmetric involvement has been occasionally reported in patients with *HSPB1* variants but was rare in our *HSPB1* patients (11%) [29]. Regarding DMs, patients with dysferlinopathies showed the highest rates of asymmetry (75%), followed by *GNE*, *MYOT*, and *ANO5* variants, findings reported by other authors [34, 35]. These conditions need to be considered in the differential diagnosis of myopathies with asymmetric involvement such as IBMs or FSHD [36].

Another feature more frequently observed in DMs was muscle hypertrophy which was found in all patients with mutations in *ANO5* and *TTN* and in most patients with variants in *DYSF, GNE, MYOT*, and *MYH7*, a finding reported elsewhere [35]. However, we also found muscle hypertrophy in some subtypes of dHMNs (*BICD2, DYNC1H1*, and *HSPB1*), a feature previously reported for *BICD2* and *DYNC1H1* but not for *HSPB1* variants [10, 11, 24].

Hyperintensities in STIR-T2w have been widely described in DMs and dHMNs [10, 37]. In our study, STIR hyperintensities appeared in a similar proportion in DMs and dHMNs, and were therefore a non-differentiating feature. While the presence of STIR hyperintensities was not discriminative between neurogenic and myogenic processes, its distribution pattern was useful in making this distinction and, to differentiate particular conditions such as anoctaminopathies or dysferlinopathies.

This study also allowed us to recognize specific patterns of muscle involvement in different genetic conditions such as *MYH7*, *ANO5*, *MYOT*, *DYSF*, and *GNE*, as reported in previous studies [17, 26, 30, 38–40]. Muscle involvement in recessive distal *TTN*-related myopathies has not been studied in depth although the involvement of the gastrocnemius, glutei and posterior thigh muscles (particularly ST) has been highlighted [41, 42]. In our cohort, fat infiltration varied considerably in patients with titinopathies, but involvement of the glutei, and TP and FHL in the legs (both commonly preserved in myopathies), with relative preservation of BFsh, were distinctive features. MRI patterns of muscle involvement in some forms of dHMN have been reported but have yet to be defined in other rarer conditions such as *SOD1* or *DNAJB2*. Our patients with *BICD2* and *HSPB1* variants showed a pattern of muscle involvement consistent with previous reports [10–12, 29]. Our study also shows the preferential involvement of the FHL and FDL in patients with *HSPB1* variants; the latter has also been reported elsewhere [10]. Patients with variants in *DYNC1H1* showed a characteristic and non-length dependent pattern of fat infiltration as previously reported [10, 24]. In patients with variants in *GARS1*, we detected fat infiltration in TA and the posterior compartment of the leg together with significant atrophy of both compartments. Despite the small number of patients with mutations in *DNAJB2* and *SOD1* in our study, we were able to observe a pattern of SL and PL involvement with preservation of thigh muscles in the early stages. Collaborative studies of larger series are needed to confirm these preliminary results.

This study has some limitations such as the disproportion between the number of patients in both cohorts, with DMs predominance over dHMNs which is not surprising given that dHMNs are rarer and have a lower rate of genetic diagnosis. Some of our conclusions could be biased by the uneven distribution of molecular subgroups, particularly the disproportionate number of patients with Laing myopathies and *ANO5* biallelic variants in the DM cohort and the significantly smaller number of patients in other subgroups, especially in the dHMNs. Finally, differences in the functional stage of patients in the different subgroups could bias the appearance of some features such as muscle islands, which are usually associated with higher degrees of fat infiltration.

Further research is needed in this field. In the future, artificial intelligence and machine learning could be used to help differentiate these conditions.

In conclusion, this study shows that certain muscle MRI features can be useful in the differential diagnosis of patients with DMs and dHMNs. A reticular pattern of fat infiltration and diffuse and significant involvement of foot intrinsic muscles are characteristic features of dHMNs. Other features, though nonspecific, are also suggestive of neurogenic conditions, such as the presence of a distal-to-proximal gradient or length-dependent pattern. Asymmetric muscle involvement and muscle hypertrophy, though nonspecific, were more common in DMs. Muscle islands predominantly occurred in dHMNs, although they were also present in up to one-third of DM patients. The degree of muscle fat replacement correlated with functional disability, and disease duration, which demonstrates the usefulness of the MRI in the evaluation of patients affected by these conditions and indicates a potential use of imaging in clinical trials.

Author Contributions

María Payá: conceptualization, data curation, formal analysis, investigation, validation, methodology, visualization, writing – original draft,

14681331, 2026, 1, Downloaded from https://onlinelibrary.wiley.com/doi/10.1111/ene.70456 by Spanish Cochrane National Provision (Ministerio de Sanidad), Wiley Online Library on [13/03/2026]. See the Terms and Conditions (https://onlinelibrary.wiley.com/terms-and-conditions) on Wiley Online Library for rules of use; OA articles are governed by the applicable Creative Commons License

review and editing. **Sofía Portela:** conceptualization, data curation, formal analysis, investigation, validation, methodology, visualization, writing – original draft, review and editing. **Rafael Sivera:** investigation, writing – review and editing. **Marina Frasquet:** investigation, writing – review and editing. **Fernando Más-Estellés:** investigation, writing – review and editing. **Pilar Martí:** investigation, writing – review and editing. **Inmaculada Azorín:** investigation, writing – review and editing. **Karolina Aragon-Gawinska:** investigation, writing – review and editing. **María Tárrega:** investigation, writing – review and editing. **Herminia Argente-Escrig:** investigation, writing – review and editing. **Juan F. Vázquez-Costa:** investigation, writing – review and editing. **Roger Vilchez:** investigation, writing – review and editing. **Juan J. Vilchez:** investigation, writing – review and editing. **Teresa Sevilla:** conceptualization, investigation, writing – review and editing. **Nuria Muelas:** conceptualization, data curation, formal analysis, investigation, validation, methodology, visualization, writing – original draft, review and editing.

Acknowledgements

We thank patients who participated in the study and their families; Grupo de Estudio de Enfermedades Neuromusculares, Sociedad Valenciana de Neurología and FA Pretel from Data Science for the statistical analysis. R.S. and T.S. are members of the inherited Neuropathy Consortium RDCRN. N.M., J.F.V.-C., R.S., and T.S. are members of the European Reference Network for Rare Neuromuscular Diseases (ERN EURO-NMD).

Funding

This study was funded by the projects PI21/01532 and PI22/01830 supported by the Instituto de Salud Carlos III (ISCIII), co-funded by the European Union. N.M. received support from the Valencian Council for Education, Culture, University and Employment (CIPROM/2023/053).

Conflicts of Interest

All authors reviewed and approved the manuscript prior to its submission. The authors declare no conflicts of interest.

Data Availability Statement

The data that support the findings of this study are available from the corresponding author upon reasonable request.

References

1. B. Udd, "Distal Myopathies - New Genetic Entities Expand Diagnostic Challenge," *Neuromuscular Disorders* 22 (2012): 5–12.

2. D. Beijer and J. Baets, "The Expanding Genetic Landscape of Hereditary Motor Neuropathies," *Brain* 143 (2020): 3540–3563.

3. M. Savarese, J. Sarparanta, A. Vihola, et al., "Panorama of the Distal Myopathies," *Acta Myologica* 39 (2020): 245–265.

4. M. Frasquet, R. Rojas-García, H. Argente-Escrig, et al., "Distal Hereditary Motor Neuropathies: Mutation Spectrum and Genotype–Phenotype Correlation," *European Journal of Neurology* 28, no. 4 (2021): 1334–1343.

5. M. Frasquet and T. Sevilla, "Hereditary Motor Neuropathies," *Current Opinion in Neurology* 35 (2022): 562–570.

6. C. J. Record, M. Pipis, M. Skorupinska, et al., "Whole Genome Sequencing Increases the Diagnostic Rate in Charcot-Marie-Tooth Disease," *Brain* 147, no. 9 (2024): 3144–3156.

7. J. Ranta-Aho, M. Johari, and B. Udd, "Current Advance on Distal Myopathy Genetics," *Current Opinion in Neurology* 37 (2024): 515–522.

8. M. Milone and T. Liewluck, "The Unfolding Spectrum of Inherited Distal Myopathies," *Muscle & Nerve* 59 (2019): 283–294.

9. E. Bugiardini, J. M. Morrow, S. Shah, et al., "The Diagnostic Value of MRI Pattern Recognition in Distal Myopathies," *Frontiers in Neurology* 9 (2018): 456.

10. D. Esteller, J. Morrow, J. Alonso-Pérez, et al., "Muscle Magnetic Resonance Imaging of a Large Cohort of Distal Hereditary Motor Neuropathies Reveals Characteristic Features Useful for Diagnosis," *Neuromuscular Disorders* 33, no. 10 (2023): 744–753.

11. A. M. Rossor, E. C. Oates, H. K. Salter, et al., "Phenotypic and Molecular Insights Into Spinal Muscular Atrophy due to Mutations in BICD2," *Brain* 138, no. 2 (2015): 293–310.

12. A. M. Rossor, J. M. Morrow, J. M. Polke, et al., "Pilot Phenotype and Natural History Study of Hereditary Neuropathies Caused by Mutations in the HSPB1 Gene," *Neuromuscular Disorders* 27, no. 1 (2017): 50–56.

13. J. R. Dahlqvist, P. Widholm, O. D. Leinhard, and J. Vissing, "MRI in Neuromuscular Diseases: An Emerging Diagnostic Tool and Biomarker for Prognosis and Efficacy," *Annals of Neurology* 88 (2020): 669–681.

14. C. Nuñez-Peralta, J. Alonso-Pérez, and J. Díáz-Manera, "The Increasing Role of Muscle MRI to Monitor Changes Over Time in Untreated and Treated Muscle Diseases," *Current Opinion in Neurology* 33, no. 5 (2020): 611–620.

15. G. Astrea, J. M. Morrow, A. Manzur, et al., "Muscle 'Islands': An MRI Signature Distinguishing Neurogenic From Myopathic Causes of Early Onset Distal Weakness," *Neuromuscular Disorders* 32, no. 2 (2022): 142–149.

16. N. Muelas, L. Carretero-Vilarroig, P. Martí, et al., "Clinical Features, Mutation Spectrum and Factors Related to Reaching Molecular Diagnosis in a Cohort of Patients With Distal Myopathies," *Journal of Neurology* 272, no. 1 (2025): 97.

17. N. Muelas, M. Frasquet, F. Más-Estellés, et al., "A Study of the Phenotypic Variability and Disease Progression in Laing Myopathy Through the Evaluation of Muscle Imaging," *European Journal of Neurology* 28, no. 4 (2021): 1356–1365.

18. D. Fischer, R. A. Kley, K. Strach, et al., "Distinct Muscle Imaging Patterns in Myofibrillar Myopathies," *Neurology* 71 (2008): 758–765.

19. E. Mercuri, B. Talim, B. Moghadaszadeh, et al., "Clinical and Imaging Findings in Six Cases of Congenital Muscular Dystrophy With Rigid Spine Syndrome Linked to Chromosome 1p (RSMD1)," *Neuromuscular Disorders* 12, no. 7–8 (2002): 631–638, https://doi.org/10.1016/s0960-8966(02)00023-8.

20. M. Garibaldi, G. Tasca, J. Diaz-Manera, et al., "Muscle MRI in Neutral Lipid Storage Disease (NLSD)," *Journal of Neurology* 264, no. 7 (2017): 1334–1342.

21. D. Esteller, M. Schiava, R. N. Villar-Quiles, et al., "Analysis of Muscle Magnetic Resonance Imaging of a Large Cohort of Patient With VCP-Mediated Disease Reveals Characteristic Features Useful for Diagnosis," *Journal of Neurology* 270, no. 12 (2023): 5849–5865.

22. J. Jiménez-Jiménez, I. Navarrete, I. Azorín, et al., "Insights Into Phenotypic Variability Caused by GARS1 Pathogenic Variants," *European Journal of Neurology* 31 (2024): e16416.

23. A. M. Rossor, B. Kalmar, L. Greensmith, and M. M. Reilly, "The Distal Hereditary Motor Neuropathies," *Journal of Neurology, Neurosurgery and Psychiatry* 83 (2012): 6–14.

24. M. Scoto, A. M. Rossor, M. B. Harms, et al., "Novel Mutations Expand the Clinical Spectrum of *DYNC1H1*-Associated Spinal Muscular Atrophy," *Neurology* 84, no. 7 (2015): 668–679, https://doi.org/10.1212/WNL.0000000000001269.

25. M. Frasquet, A. Camacho, R. Vílchez, et al., "Clinical Spectrum of BICD2 Mutations," *European Journal of Neurology* 27, no. 7 (2020): 1327–1335.

26. G. Tasca, E. Ricci, M. Monforte, et al., "Muscle Imaging Findings in GNE Myopathy," *Journal of Neurology* 259, no. 7 (2012): 1358–1365.

14681331, 2026, 1, Downloaded from https://onlinelibrary.wiley.com/doi/10.1111/ene.70456 by Spanish Cochrane National Provision (Ministerio de Sanidad), Wiley Online Library on [13/03/2026]. See the Terms and Conditions (https://onlinelibrary.wiley.com/terms-and-conditions) on Wiley Online Library for rules of use; OA articles are governed by the applicable Creative Commons License

27. E. Gallardo, A. García, O. Combarros, and J. Berciano, "Charcot-Marie-Tooth Disease Type 1A Duplication: Spectrum of Clinical and Magnetic Resonance Imaging Features in Leg and Foot Muscles," *Brain* 129, no. 2 (2006): 426–437.

28. C. M. Doherty, P. Howard, L. F. O'Donnell, et al., "Quantitative Foot Muscle Magnetic Resonance Imaging Reliably Measures Disease Progression in Children and Adolescents With Charcot–Marie–Tooth Disease Type 1A," *Annals of Neurology* 96, no. 1 (2024): 170–174.

29. M. Gaeta, A. Mileto, A. Mazzeo, et al., "MRI Findings, Patterns of Disease Distribution, and Muscle Fat Fraction Calculation in Five Patients With Charcot-Marie-Tooth Type 2 F Disease," *Skeletal Radiology* 41, no. 5 (2012): 515–524.

30. A. M. S. Silva, A. R. Coimbra-Neto, P. V. S. Souza, et al., "Clinical and Molecular Findings in a Cohort of ANO5-Related Myopathy," *Annals of Clinical Translational Neurology* 6, no. 7 (2019): 1225–1238.

31. B. Ansari, E. Salort-Campana, A. Ogier, et al., "Quantitative Muscle MRI Study of Patients With Sporadic Inclusion Body Myositis," *Muscle & Nerve* 61, no. 4 (2020): 496–503.

32. G. Tasca, M. Monforte, J. Díaz-Manera, et al., "MRI in Sarcoglycanopathies: A Large International Cohort Study," *Journal of Neurology, Neurosurgery, and Psychiatry* 89, no. 1 (2018): 72–77.

33. J. Díaz-Manera, G. Walter, and V. Straub, "Skeletal Muscle Magnetic Resonance Imaging in Pompe Disease," *Muscle & Nerve* 63 (2021): 640–650.

34. I. Mahjneh, R. Bashir, S. Kiuru-Enari, W. Linssen, A. Lamminen, and M. Visser, "Selective Pattern of Muscle Involvement Seen in Distal Muscular Dystrophy Associated With Anoctamin 5 Mutations: A Follow-Up Muscle MRI Study," *Neuromuscular Disorders* 22, no. SUPPL. 2 (2012): S130–S136.

35. L. ten Dam, A. J. van der Kooi, F. Rövekamp, W. H. J. P. Linssen, and M. de Visser, "Comparing Clinical Data and Muscle Imaging of DYSF and ANO5 Related Muscular Dystrophies," *Neuromuscular Disorders* 24, no. 12 (2014): 1097–1102.

36. L. Llansó, U. Moore, C. Bolano-Diaz, et al., "Expanding the Muscle Imaging Spectrum in Dysferlinopathy: Description of an Outlier Population From the Classical MRI Pattern," *Neuromuscular Disorders* 33, no. 4 (2023): 349–357.

37. S. Holm-Yildiz, N. Witting, B. J. de Stricker, et al., "Muscle Biopsy and MRI Findings in ANO5-Related Myopathy," *Muscle & Nerve* 64, no. 6 (2021): 743–748, https://doi.org/10.1002/mus.27419.

38. J. Vazquez, C. Lefeuvre, R. E. Escobar, et al., "Phenotypic Spectrum of Myopathies With Recessive Anoctamin-5 Mutations," *Journal of Neuromuscular Diseases* 7, no. 4 (2020): 443–451.

39. N. Schramm, C. Born, S. Weckbach, P. Reilich, M. C. Walter, and M. F. Reiser, "Involvement Patterns in Myotilinopathy and Desminopathy Detected by a Novel Neuromuscular Whole-Body MRI Protocol," *European Radiology* 18, no. 12 (2008): 2922–2936.

40. J. Díaz, L. Woudt, L. Suazo, et al., "Broadening the Imaging Phenotype of Dysferlinopathy at Different Disease Stages," *Muscle & Nerve* 54, no. 2 (2016): 203–210.

41. E. C. Oates, K. J. Jones, S. Donkervoort, et al., "Congenital Titinopathy: Comprehensive Characterization and Pathogenic Insights," *Annals of Neurology* 83, no. 6 (2018): 1105–1124.

42. B. Udd, "The Constantly Evolving Spectrum of Phenotypes in Titinopathies—Will It Ever Stop?," *Current Opinion in Neurology* 33 (2020): 604–610.

Supporting Information

Additional supporting information can be found online in the Supporting Information section. **Appendix S1:** MRI pattern description by genes affected. **Table S1:** Detailed description of clinical data, pathogenic variants, and main muscle MRI findings in each patient. **Table S2:** Muscle fat replacement based on Mercuri score for each patient of the study. The top row shows the muscles evaluated. The mean Mercuri Score was calculated for each anatomic segment including the leg (Sum leg), thigh (Sum thigh), and pelvis (Sum pelvis) separately. The mean Mercuri score of all muscles involved was also calculated for each patient (Sum total or whole cumulative score [WCS]). **Table S3:** Mean Mercuri score of muscles of the lower leg, thigh and pelvis in the DM and dHMN cohorts. **Table S4:** Distribution of muscle islands.

14681331, 2026, 1, Downloaded from https://onlinelibrary.wiley.com/doi/10.1111/ene.70456 by Spanish Cochrane National Provision (Ministerio de Sanidad), Wiley Online Library on [13/03/2026]. See the Terms and Conditions (https://onlinelibrary.wiley.com/terms-and-conditions) on Wiley Online Library for rules of use; OA articles are governed by the applicable Creative Commons License